Materials and Design 45 (2013) 72–79

Contents lists available at SciVerse ScienceDirect

Materials and Design

journal homepage: www.elsevier.com/locate/matdes

The microstructure and mechanical properties of fluxless gas tungsten arc welding–brazing joints made between titanium and aluminum alloys

Zhipeng Ma, Changwen Wang, Hanchen Yu, Jiuchun Yan *, Haoran Shen

State Key Laboratory of Advanced Welding Production Technology, Harbin Institute of Technology, Harbin 150001, PR China

ARTICLE INFO

Article history:
Received 9 June 2011
Accepted 3 September 2012
Available online 12 September 2012

Keywords:
A. Non-ferrous metals and alloys
D. Bonding
F. Microstructure

ABSTRACT

Butt joining of a titanium alloy to an aluminum alloy by gas tungsten arc welding–brazing using an Al-Si eutectic filler wire without flux is investigated. The butt joints have dual characteristics, being a welding on the aluminum side and a brazing on the titanium side. The thickness of the reaction layer varies with position in the titanium alloy interfacial area of the joint, ranging from 2 to 5 μm. At the upper part of interfacial area, the reaction layer includes only the rod-like $TiAl_3$ phase with 10 at.% dissolved Si. At the bottom of interfacial area, the reaction layer consists of the needle-like τ1 phases ($Ti_7Al_5Si_{12}$) and the block-like $TiAl_3$ phase. Hardness of the reaction layer near the welded seam/Ti alloy interface was as much as 400–500 HV. The highest tensile joint strength observed was 158 MPa. Tensile joint failure was by cracks initiating from the reaction layer at the bottom of the joint propagating into the welded seam at the upper part of the joint.

1. Introduction

Aluminum (Al) and titanium (Ti) alloys are used in industry to reduce weight and improve strength. As a result, various joining processes have been developed to bond aluminum alloys to titanium alloys. Examples are laser welding–brazing [1], friction bonding [2,3], friction stir bonding [4], diffusion bonding [5,6], brazing [7] and transient liquid phase bonding [8]. Unfortunately, Al and Ti alloys cannot be joined successfully using conventional gas tungsten arc (GTA) welding due to differences in the physical, chemical and metallurgical properties of the base metals. These differences result in the formation of large quantities of brittle intermetallic compounds that seriously degrade the mechanical properties of the joints: there is still much fundamental work to be done to find optimum process parameters. Tungsten inert gas welding–brazing of aluminum alloy–steel butt joints [9,10] has been accomplished, and this method has great potential to prevent the dissolution of steel into the weld metal so that a continuous joint can be made by the deposition of fused filler metal without the melting the base metal. For joining Ti/Al, previous studies [11] have mainly focused on laser welding–brazing with a flux-cored wire. The presence of flux improves the wetting and spreading of liquid filler metal on the Ti surface, but after welding, the residual flux deposits on the surface of base metal near the welded seam are very difficult to remove. However, without flux, the liquid filler metal will not wet or spread on the Ti surface during dynamic arc heating. To date, little has been published on fluxless Ti/Al GTA welding–brazing.

In this study, Ti/Al GTA welding–brazing joints were made successfully without any flux. The macrostructure and microstructure of the joints were analyzed and the mechanical and fracture properties were evaluated.

2. Experimental procedure

The materials used were 2024-T6 aluminum alloy and Ti–6Al–4V titanium alloy in 3 mm sheet form. The 2.5 mm diameter filler wire was 4047 Al–12Si alloy. No flux was present in the filler wire and none was added externally. The nominal chemical compositions of the base materials and filler wire are shown in Table 1.

All sheets were cut into nominal 100 × 50 mm samples, a 30° bevel was cut on one long edge of each sample, and the surface was cleaned using abrasive paper and acetone. To make the test joints, two samples were butted together, with the two beveled edges forming a groove. GTA welding–brazing was done using an AC-GTA welding source. The welding parameters were 70–150 A current, giving an arc length of 3.0–4.0 mm. The welding speed was 75 mm/min with an argon gas flow rate of 10 L/min.

After welding, a typical cross-section of the joint was cut and mounted in self-setting epoxy resin in an as-clamped condition. Then the metallographic samples were polished to a mirror-like surface aspect and etched for 10 s in a single batch using Keller's reagent. The macrostructure of the joint was investigated using optical microscopy (OM, Olympus PM-20) and the microstructure of reaction layer were measured by scanning electron microscopy

* Corresponding author. Tel.: +86 451 86416607; fax: +86 451 86416186.
E-mail address: jcyan@hit.edu.cn (J. Yan).

0261-3069/$ - see front matter © 2012 Elsevier Ltd. All rights reserved.
http://dx.doi.org/10.1016/j.matdes.2012.09.007

Table 1
Chemical compositions (wt.%) of 2024 aluminum alloy, Ti–6Al–4V titanium alloy and filler wire.

Constituent	Mn	Cu	Mg	V	Fe	Ti	Si	Al	Zn
Ti–6Al–4V	–	–	–	3.60	0.30	Bal.	–	6.21	–
2024	0.80	3.90	1.40	–	0.14	0.15	0.55	Bal.	0.27
Filler wire	<0.05	<0.30	<0.10	–	<0.80	0.77	11.0–13.0	Bal.	<0.20

(SEM, FEI Quanta 200F) with energy dispersive spectrometer (EDS) used for local chemical analysis. The interfacial reactants in the joint were identified by selected area diffraction pattern (SADP) in the transmission electron microscope (TEM, FEI Tecnai F30). TEM specimens were prepared with cutting, grinding and ion milling to electron transparency. Thin sheets (8 mm × 8 mm × 0.3 mm) were cut from brazing zone where the interface reaction zone was approximately located in midline by a linear cutting machine. The thin sheets were thinned down into parallel sided and semi-thin sheets with thicknesses of around 50 μm through several steps of coarse grinding, fine grinding and mechanical polishing. The semi-thin sheets were then cut into 3 mm discs. Ion milling was performed on both sides of the specimens with two beams of 4 kV Ar ions by using a Gatan 691 Ion-Miller. After repeated attempts, the specimens with electron transparency at reaction layer have been achieved.

The microhardness of the welded specimens was determined by a Vickers hardness tester (Akashi HM-102) under a load of 200 g for 10 s dwell time ($HV_{0.2}$/10). The tests were carried out on three randomly selected points in every measurement region, and the average value was employed as the test result. Tensile strengths of the Ti/Al joints were carried out on full-width strips (15 × 98 mm) at a constant speed of 1 mm/min using an Instron 5569 tensile testing machine at room temperature. Under the condition of the same welding parameters, three specimens were fabricated for the tensile test, and then average values of the tensile strength were obtained. In order to evaluate the tensile strengths of these samples accurately and avoid the influence of the excess weld metal on joining strength, the joints were ground to be flat.

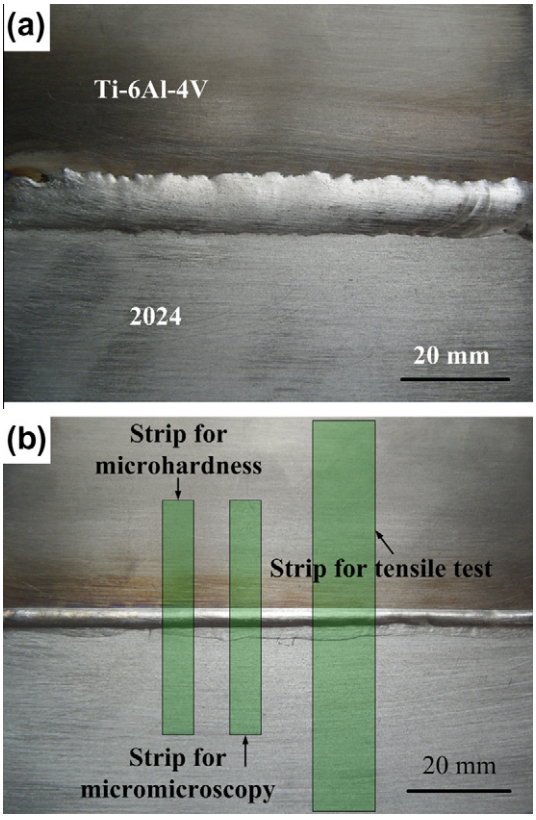

Fig. 1. Typical weld appearances of the Ti/Al GTA welding–brazing joint: (a) top and (b) underside.

3. Results and discussion

3.1. Weld appearance

Fig. 1 shows the typical appearance of a Ti/Al GTA welding–brazing joint. It is clear that the surface of the joint is smooth, and the Ti alloy has been well wetted by the filler giving a consistent joint on both sides. No cracks were observed on the interface between the welded seam and Ti alloy, nor were undercuts or incomplete fusion observed in Al alloy side. Internal defects such as cold shuts were not observed giving an early indication the joints are sound. The test region is 60 mm long and 94 mm wide, Fig. 1b shows the specimen cutting patterns.

3.2. Macrostructure

The effects of the welding current on the joint characteristics are shown in Fig. 2. At 100 A welding current, the filler metal only spreads on Ti alloy surface, which does not melt at all, as shown in Fig. 2a. There is a narrow range of optimum welding currents of 110–120 A, in this range, the filler metal spreads fully on the Ti alloy surface to form a sound joint. The joint has the typical welding–brazing dual characteristics (see Fig. 2b). The Al alloy base metal melts and is thus a welded joint, and the molten Al mixes with the molten filler metal to form fusion area. The Ti alloy base metal does not melt and is thus a brazed joint, where wetting with the molten filler metal forms the brazing interface layer. We have observed some isolated micro-pores (<0.2 mm) or short chains of micro-pores in the welded seam close to the Al alloy side. Such pores are very common in GTA welding of Al alloy, and are caused by entrapped gaseous impurities, as shown in Fig. 2c and d. By increasing the welding current to 130 A, the upper part of the Ti alloy groove melts and cracking occurs in the welded seam nearly perpendicular to the interface after welding due to the formation of significant quantities of intermetallic compounds.

3.3. Microstructure

Liquid filler metal has fully spread on the Ti alloy surface to form a good surface. The mixing of the Ti alloy and the melting filler metal is effectively avoided when GTA welding–brazing. Furthermore, the formation of the intermetallic compounds at the interface is controlled, as shown in Fig. 3a. The welded seam, as shown in Fig. 3b, has a mainly dendritic structure. The micrographs clearly show a-Al grains, granular Si and compound Mg_2Si [12]. As shown in Fig. 3c, there are four different zones: the base metal, a heat affected zone (HAZ), a fusion zone (FZ) and the welded seam. The dendritic structure in the welded seam is nearly perpendicular to the fusion line, being induced by the higher cooling rate and the direction of conductive heat flow during cooling. During the welding process, a fusion zone was formed by melting the Al alloy and

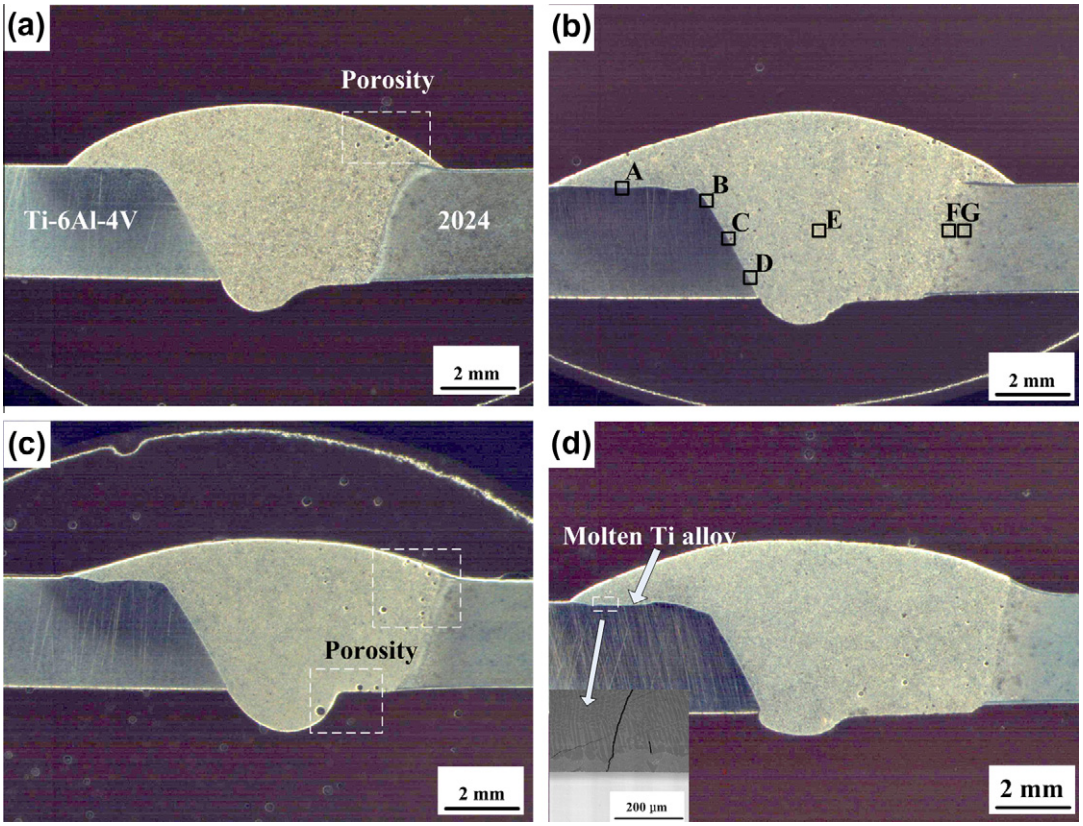

Fig. 2. Macroscopic cross-section of Ti/Al GTA welding–brazing joints made with varying welding currents (a) 100 A, (b) 110 A, (c) 120 A and (d) 130 A.

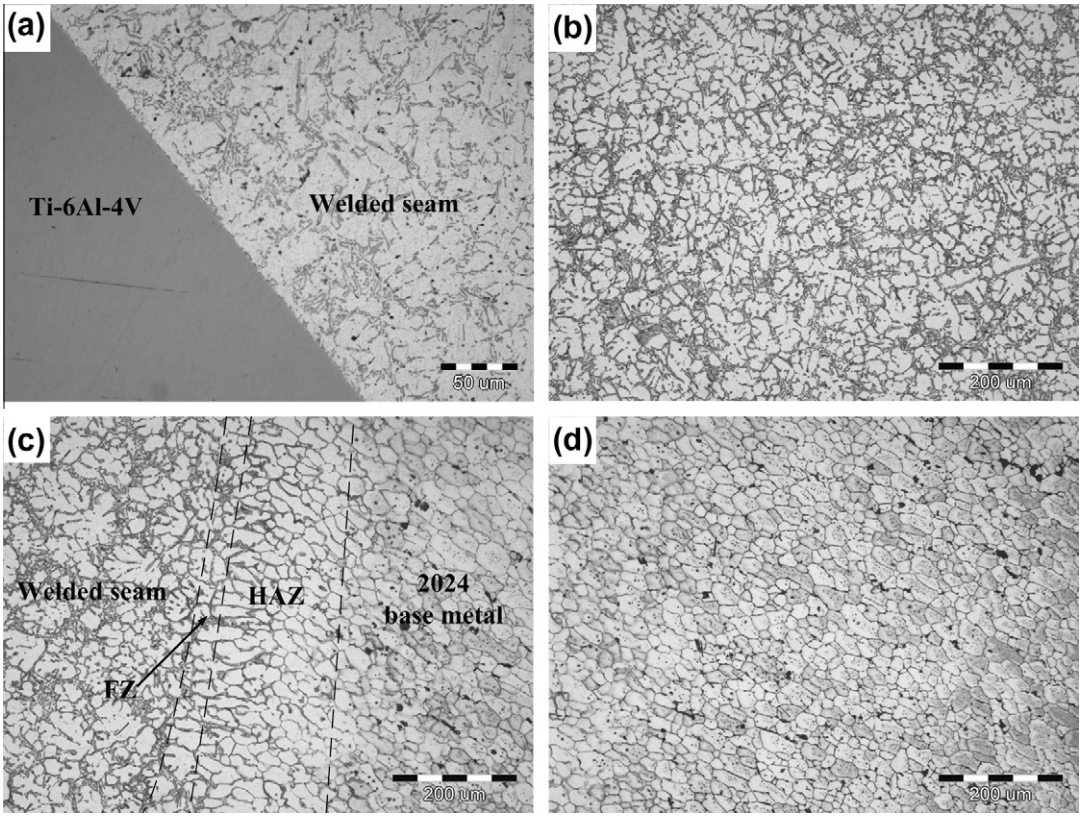

Fig. 3. Microstructure of the Ti/Al GTA welding–brazing joint (a) at the interfacial zone close to Ti alloy (taken in the area marked by rectangle C in Fig. 2b), (b) at welded seam in Fig. 2b alloy (taken in the area marked by rectangle E in Fig. 2b), (c) at fusion zone of aluminum alloy (taken in the area marked by rectangle F in Fig. 2b), and (d) at base metal of aluminum alloy (taken in the area marked by rectangle G in Fig. 2b).

the filler metal. It is likely that diffusion of elemental Si in the molten pool into fusion zone induced the formation of the ternary hypoeutectic structure with Al, Si and Mg_2Si. The equiaxed crystal structure in the heat affected zone is similar to that in base metal and in the partially molten Al alloy matrix mixed with the completely melted filler metal. Fig. 3d shows the microstructure of the Al alloy base metal.

Heat input has an important influence on interfacial reaction mechanisms in GTA welding–brazing, inducing an uneven distribution of reaction layer morphologies. Fig. 4a–d shows interfacial microstructure micrographs of the rectangular regions labeled A-D in Fig. 2b. At A and B (Fig. 4a and b), the thickness of the interfacial reaction layer is approximately 4 μm. EDS results indicate that the reaction layer is composed of a $TiAl_3$ phase with 11 at.% dissolved Si (see Table 2). The results are consistent with those of the reaction between solid Ti and liquid Al seen in previous studies [13,14]. The microstructure of the reaction layer shows that it is made up of numerous rod-like $TiAl_3$ grains. In zone C (Fig. 4c), the thickness of the interfacial reaction layer is approximately 2 μm and the microstructure exhibits a compact continuous morphology, compositional analysis shows it to be a $TiAl_3$ phase with 10 at.% dissolved Si (see Table 2). In zone D, the thickness of the needle-like and block-like interfacial reaction layers adjacent to the Ti alloy side is about 2 μm. The EDS results indicate that Si atoms gather at the interface and participate in the formation of the needle-like interfacial reaction layer. Compared with ternary alloy phase diagrams of typical Ti–Al–Si systems taken from previous studies [15], the needle-like interfacial reactant is τ1 phase ($Ti_7Al_5Si_{12}$).

Table 2
EDS analysis results of interfacial reaction layer in Fig. 5 (at.%).

at.%	Al	Ti	Si	V	Phase
A	72.36	16.12	11.40	0.12	$Ti(Al,Si)_3$
B	78.35	8.37	13.11	0.17	$Ti(Al,Si)_3$ + Al
C	63.31	24.86	11.18	0.64	$Ti(Al,Si)_3$
D	61.91	26.81	10.44	0.84	$Ti(Al,Si)_3$
E	53.97	20.16	25.46	0.41	τ1 + $Ti(Al,Si)_3$ + Al

To further identify the phase structures of the reaction layers, line scanning of the interfacial layer was carried out, see Fig. 5a–c. Line scan analysis from the welded seam toward the inside of Ti alloy shows that the Al content falls and the Ti content rises sharply to a constant level. Then the Al content drops significantly to 6–8 wt.% whilst Ti content increases. The results of the EDS line scans indicate that Si atoms are concentrated in the interface because Ti dissolution induces the decrease of the Si chemical potential. According to corresponding SADP, block-like reactant has been identified as $TiAl_3$, and needle-like reactant has been identified as τ1 (see Fig. 5d and e). In zones A and B, the solubility of Si in the $TiAl_3$ phase rises up to about 11 at.%. The reaction layer close to Ti alloy is composed of the $Ti(Al,Si)_3$ phase. In zone C, a mass of Si atoms are found at the interface, and τ1 phase is formed. The reaction layer consists of the $Ti(Al,Si)_3$ and τ1 phases.

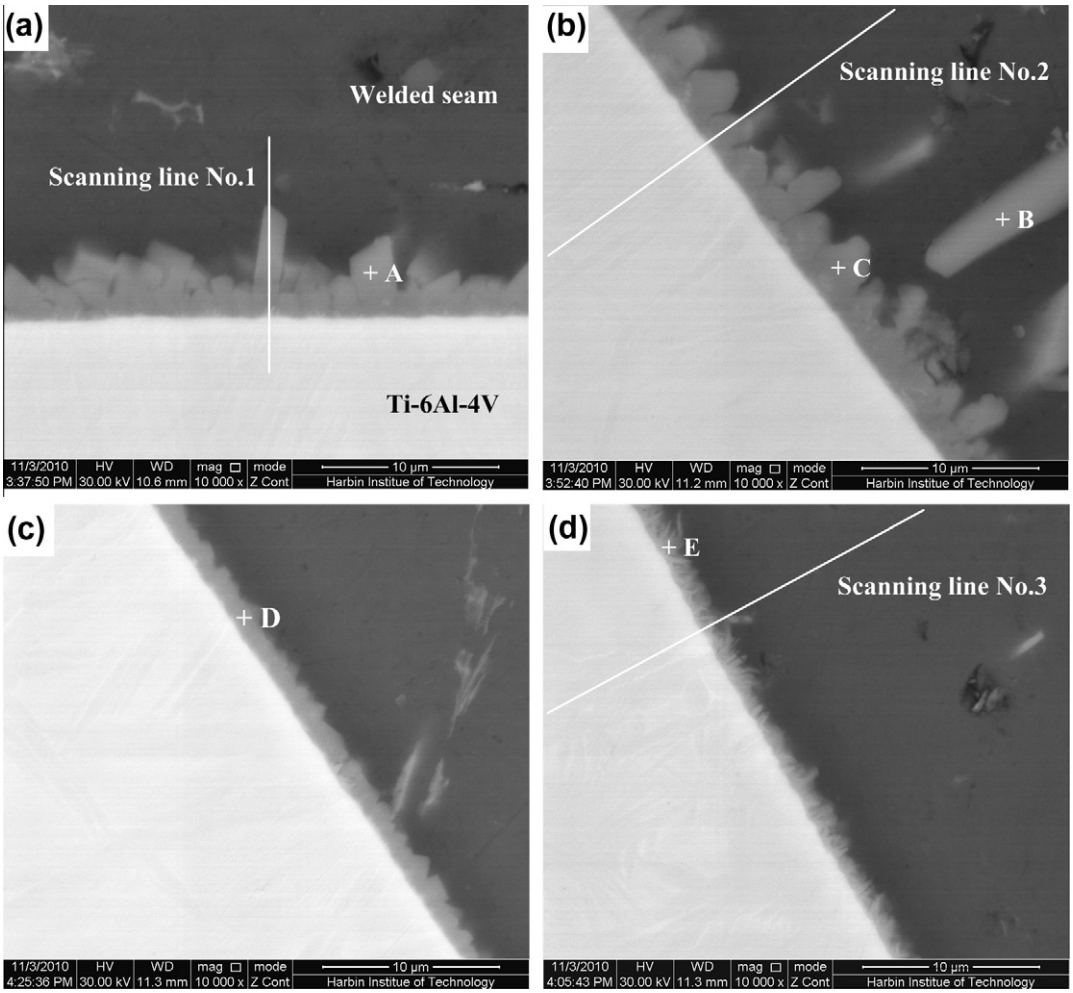

Fig. 4. Microstructure of interfacial reaction layer: (a–d) magnified micrographs of regions taken from the areas marked by rectangles A–D in Fig 2b, respectively.

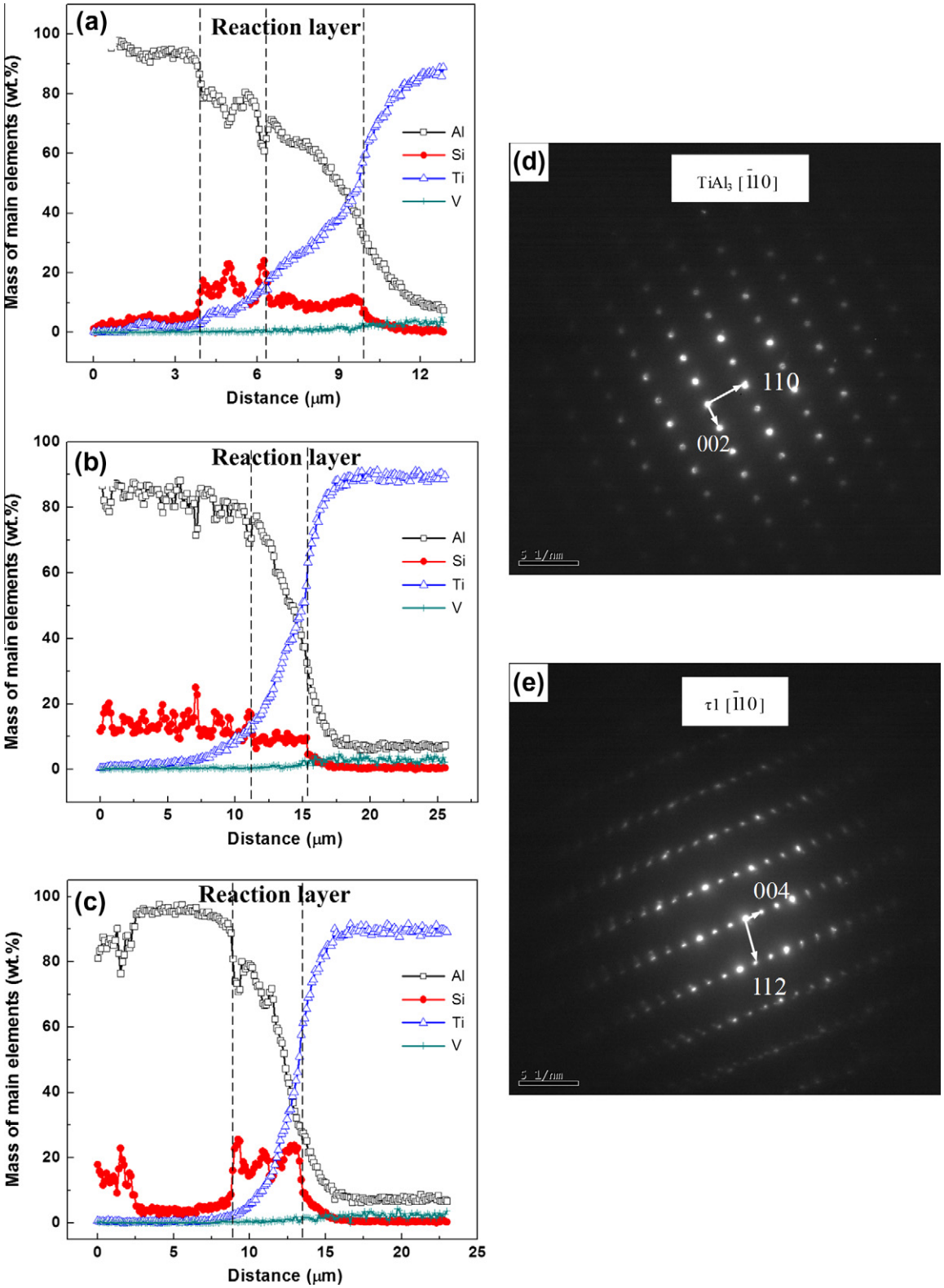

Fig. 5. Line scans and corresponding SADP taken in the interfacial layer: (a–c) the positions of scanning lines 1–3 are shown in Fig. 4, (d) corresponding SADP of $TiAl_3$ phase and (e) corresponding SADP of τ1 phase.

Non-uniform heating is a disadvantage to melt filler wire stably and wet base metals in GTA welding. Fluxes are generally used in welding to remove oxides from the base metal surface by a reduction and dissolution reaction, to protect the clean surface from reoxidation, and to modify the surface tension of the molten metal [16]. But the residual flux deposits on the surface of base metal near the welded seam are very difficult to remove. To avoid this shortcoming, bonding of Al alloy and Ti alloy was achieved by GTA welding–brazing without the use of flux. Arc heating provides high energy density; actually, temperature of the Ti alloy base

metal at the interface rapidly increases above 1273 K. When the hot surface of the Ti alloy comes in contact with the molten filler metal due to arc pressure, the latter melts and spreads along the surface of the Ti alloy before reoxidation. This situation leads to solid–liquid interaction and accelerates the diffusion of Ti atoms in molten filler metal. Simultaneously, diffusion of a large number of Ti atoms in liquid filler metal can cause formation of $TiAl_3$ phase on the Ti alloy side of the joint [17,18,13]. But only a small amount of brittle $TiAl_3$ phase formed on the Ti alloy side of the joint because the thermal cycle of arc heating provides a condition that is far away from thermodynamic equilibrium. The thickness of the interfacial reaction layer containing $TiAl_3$ phase is only 4 μm.

In the paper, an Al–12Si filler metal is used for GTA welding–brazing. Besser et al. [19] found that Si produces a great retardation effect on the Ti/Al reaction, and proposed that this effect is due to several mechanisms that involve diffusion and incorporation of Si into the growing $TiAl_3$ phase. According to the first-principles study [20], Si atoms have a clear preference to substitute Al atoms due to the energy stabilization effect. The $TiAl_3$ phase can dissolve Si up to 12.5 – 18.75 at.%, and become the $Ti(Al,Si)_3$ phase. Additional Si content can result in the reaction between the $Ti(Al,Si)_3$ phase and Si, and form the τ1 phase [21]. It can be observed in the bottom part of the joint that the formation of brittle $TiAl_3$ phase is suppressed and that of the τ1 phase is promoted. The results show that if sound joints are to be manufactured it is very important to clarify the effect of heat input. In a narrow range of welding currents (110–120 A), the filler metal spread fully on Ti alloy surface to form a sound joint with the typical dual characteristics of the welding–brazing process.

3.4. Hardness

Results of hardness measurements taken on the Ti/Al GTA welding–brazing joint made with a welding current of 110 A are shown in Fig. 6. Hardness on the Ti alloy side remains nearly constant (320 HV). The graph shows that the hardness of the Ti alloy is significantly higher than that of welded seam (95 HV). Fig. 7 shows hardness distributions along the joint. For the reaction phase, the hardness is very difficult to measure in such a thin layer. The technique used requires the sample to be tilted at a small angle to produce magnified reaction by increasing the apparent thickness of the layer. The reaction layer shows continuous higher hardness levels (400–500 HV) near the welded seam/Ti alloy interface, because of the formation of the $Ti(Al,Si)_3$ phases and the τ1 phase.

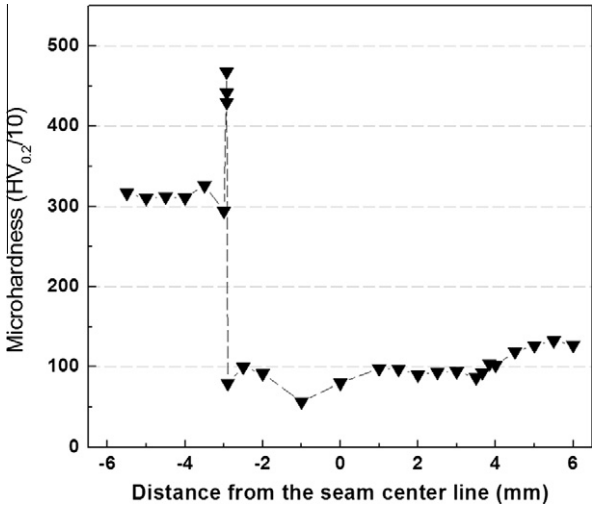

Fig. 6. Hardness variation in the Ti/Al GTA welding–brazing joint welded at 110 A.

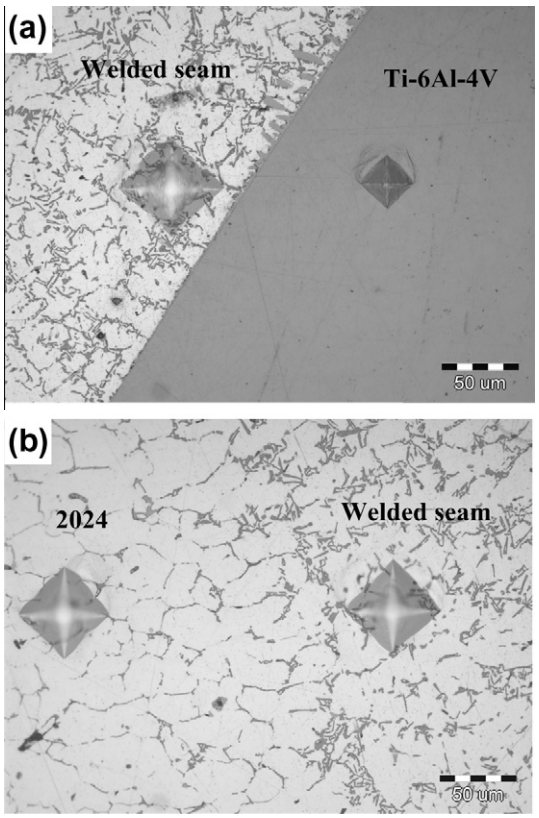

Fig. 7. Hardness distributions along the joint (a) at interfacial zone close to Ti alloy and (b) at the fusion zone close to the Al alloy.

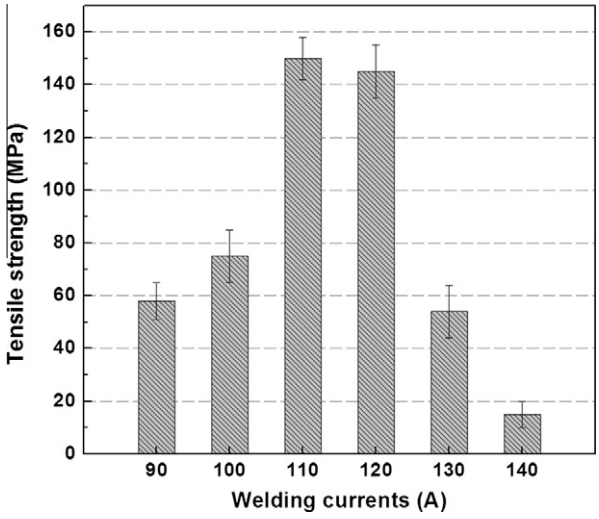

Fig. 8. Variation of the tensile strength of Ti/Al GTA welding–brazing joints with welding current.

From previous work [22], the single $TiAl_3$ phase is hard, measuring 600–700 HV. Thus the hardness of the reaction layer is attributed to the presence of the dispersive soft Al phase and a certain degree replacement of Al atoms by Si atoms in the $TiAl_3$ phase. The original hardness of 2024-T6 aluminum alloy is about 140 HV, but in the heat effected zone the average hardness is slightly reduced to 118 HV. The softened heat effect zone is reduced due to lower heat input, and this is beneficial to the mechanical properties of the joint. Commonly initial precipitates are dissolved and replaced by

other constituents. In 2024 Al alloy, Mg, Si and Cu are the elements contributing to hardening the Mg_2Si phase and the $Al_5Cu_2Mg_8Si_6$ phases [23].

3.5. Strength and fracture

To evaluate accurately the tensile strength of these samples and avoid the influence of excess weld metal, the test joints were ground flat. Fig. 8 shows how tensile strength varies with welding current. The Ti/Al joint welded at 110 A reaches the maximum tensile strength of 158 MPa.

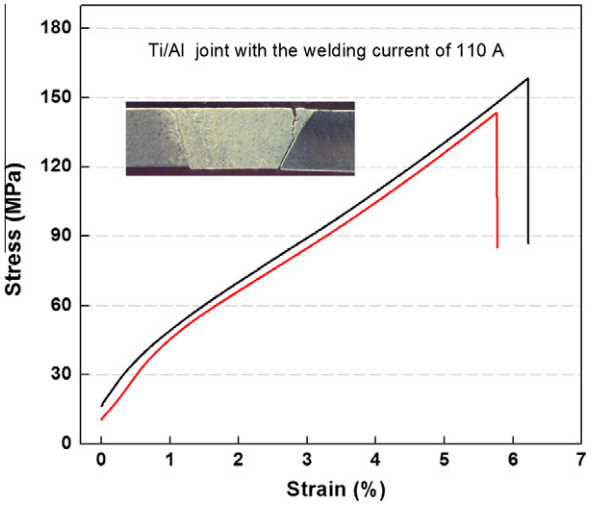

Fig. 9. Tensile stress–strain curves for joints welded at 110 A.

Fig. 9 shows stress–strain curves obtained from tensile tests for joints welded at 110 A. The fracture of a 110 A Ti/Al joint occurred at the interfacial layer close to the Ti alloy and the inside of the welding seam. Microscopy was used to determine the crack path and failure mode, because the actual crack path influences the strength of the joint. Fig. 9 shows the corresponding path of cracks in the joint. According to these observations, the fracture mechanism of the Ti/Al joint is proposed. The fracture initiates from the root interfacial layer of the joint and propagates in the welded seam, which is in the weakest zone containing porosities. The reason for this may be the $TiAl_3$ present in the interfacial layer, where the stress concentration is maximal due to the root geometry. The $TiAl_3$ phase, with a tetragonal DO_{22} structure [24], is characterized by extreme brittleness and becomes a source of internal microcracks originating during loading. The results show that the crack initiates from the reaction layer at the bottom of the joint and extends into the welded seam at the upper part of the joint. Fig. 10 shows fracture surface of Al alloy side of the joint. The fractured surfaces also reveal a quasi-cleavage fracture, and that the brittleness of the joints is due to the fracture path through the reaction layer, as shown in Fig. 10b. It is clear that many micro tear ridges, induced by the metal welding seam, appear at the fracture surface (Fig. 10c).

When welding at 90 A, the liquid filler metal spreads on the surface of Ti alloy, but does not effectively wet the Ti alloy or seam due to the low heat input. Most specimens break in the interface layer. When the welding current is increased to 140 A, the upper part of the Ti alloy groove is molten and cracking happens at the interfacial reaction zone after welding due to the high heat input (Fig. 11a). Significant amounts of intermetallic compounds are present in the welded seam (Fig. 11b), which is prone to crack at high loads.

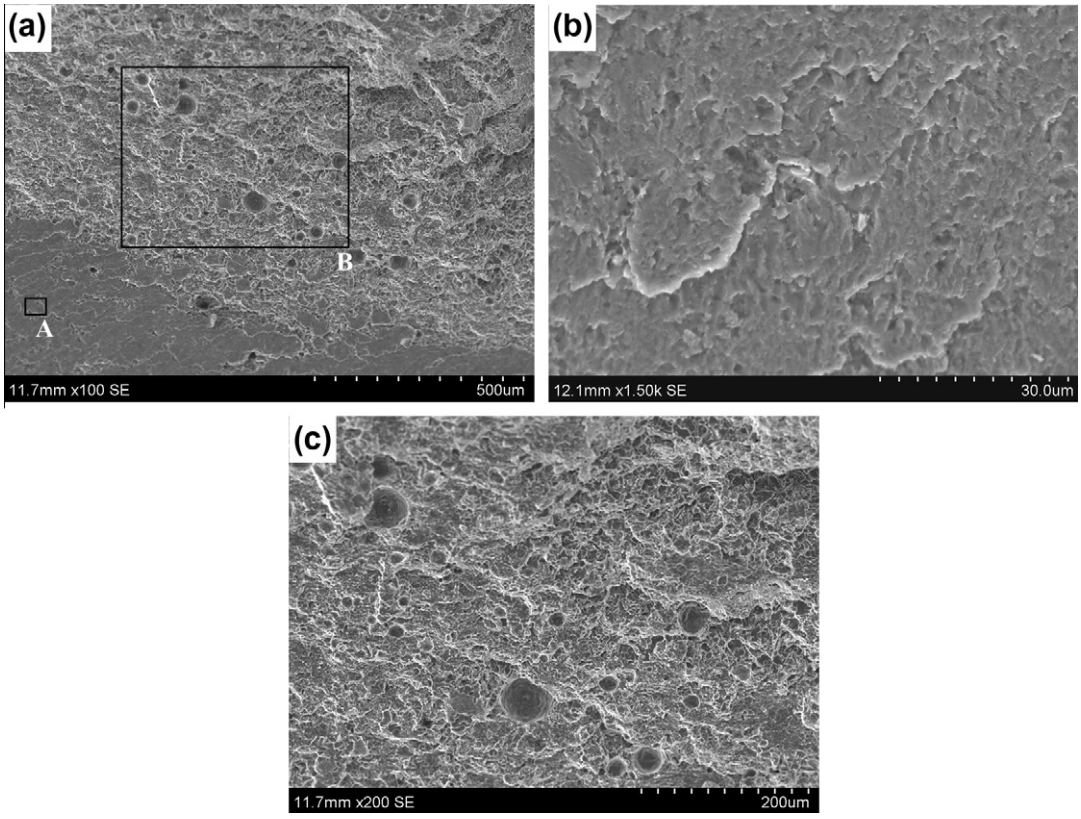

Fig. 10. Fracture surfaces of the joints welded at 110 A: (a) at the fracture surface of Al alloy side of the joint. (b and c) are magnified images taken from the zones marked A and B in Fig. 10(a).

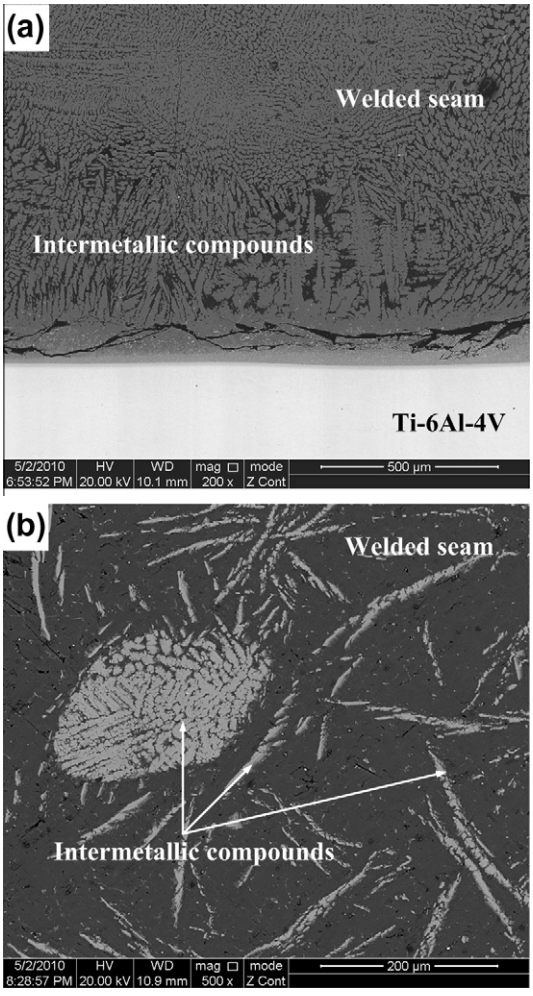

Fig. 11. Microstructure of interfacial reaction layer of a joint welded at 140 A: (a) at the interfacial zone close to Ti alloy and (b) at the welded seam.

4. Conclusions

Joining coupons of 2024 and Ti–6Al–4V was achieved by GTA welding–brazing without the use of flux. The titanium alloy base metal does not melt and reacts with the molten filler metal to form non-uniform reaction layer at the titanium alloy interfacial area of the joint. The thickness of the reaction layer ranges from 2 μm to 5 μm. At the top part of interfacial area, the reaction layer includes only a rod-like $TiAl_3$ phase with 10 at.% Si solubility. At the bottom part of interfacial area, the reaction layer is composed of needle-like τ1 phases ($Ti_7Al_5Si_{12}$) and the block-like $TiAl_3$ phase. The growth mechanism of the reaction layer is controlled by the dissolution and diffusion of Ti atoms in the molten filler metal. Elemental Si concentrates at the titanium alloy interfacial area. It is found that the diffusion behavior of Si has a significant effect on the formation of the reaction layer. The maximum joint tensile strength observed was 158 MPa, greater than 60% of the tensile strength of the aluminum alloy base metal. During tensile failure cracks initiate from the reaction layer at the bottom of the joint and propagate into the welded seam at the upper part of the joint.

Acknowledgement

This research is supported by the National Natural Science Foundation of China (No. 51075104 and No. 50975054).

References

[1] Chen YB, Chen SH, Li LQ. Influence of interfacial reaction layer morphologies on crack initiation and propagation in Ti/Al joint by laser welding–brazing. Mater Des 2010;31:227–33.
[2] Fuji A, Ameyama K, North TH. Influence of silicon in aluminum on the mechanical-properties of titanium/aluminium friction joints. J Mater Sci 1995;30:5185–91.
[3] Fuji A, Kimura M, North TH, Ameyama K, Aki M. Mechanical properties of titanium–5083 aluminium alloy friction joints. Mater Sci Technol 1997;13:673–8.
[4] Chen YC, Nakata K. Microstructural characterization and mechanical properties in friction stir welding of aluminum and titanium dissimilar alloys. Mater Des 2009;30:469–74.
[5] Sohn WH, Bong HH, Hong SH. Microstructure and bonding mechanism of Al/Ti bonded joint using Al–10Si–1Mg filler metal. Mater Sci Eng A 2003;355:231–40.
[6] Yao W, Wu AP, Zou GS, Ren JL. Formation process of the bonding joint in Ti/Al diffusion bonding. Mater Sci Eng A 2008;480:456–63.
[7] Takemoto T, Okamoto I. Intermetallic compounds formed during brazing of titanium with aluminium filler metals. J Mater Sci 1988;23:1301–8.
[8] AlHazaa A, Khan TI, Haq I. Transient liquid phase (TLP) bonding of Al7075 to Ti–6Al–4V alloy. Mater Charact 2010;61:312–7.
[9] Lin SB, Song JL, Yang CL, Ma GC. Metallurgical and mechanical investigations of aluminium–steel butt joint made by tungsten inert gas welding–brazing. Sci Technol Weld Joining 2009;14:636–9.
[10] Lin SB, Song JL, Yang CL, Fan CL, Zhang DW. Brazability of dissimilar metals tungsten inert gas butt welding–brazing between aluminum alloy and stainless steel with Al–Cu filler metal. Mater Des 2010;15:213–8.
[11] Chen SH, Li LQ, Chen YB. Interfacial reaction mode and its influence on tensile strength in laser joining Al alloy to Ti alloy. Mater Sci Technol 2010;26:230–5.
[12] Chen SH, Li LQ, Chen YB, Huang JH. Joining mechanism of Ti/Al dissimilar alloys during laser welding–brazing process. J Alloys Compd 2011;509:891–8.
[13] Sujata M, Bhargava S, Sangal S. On the formation of $TiAl_3$ during reaction between solid Ti and liquid Al. J Mater Sci Lett 1997;16:1175–8.
[14] Abdel-Hamid AA. Hot dip aluminide coating of Ti and the effect of impurities and alloying additions in the molten Al bath. Z. Metallkd 1991;82:921–7.
[15] Qin QD, Zhao YG, Liu C, Zhou W, Jiang QC. Development of aluminium composites with in situ formed AlTiSi reinforcements through infiltration. Mater Sci Eng A 2007;460–461:604–10.
[16] Olson DL, Siewert TA, Liu S, Edwards GR. Welding, brazing and soldering. ASM Handbook, vol. 6. ASM International; 1993.
[17] Peng LM, Wang JH, Li H, Zhao JH, He LH. Synthesis and microstructural characterization of Ti–Al_3Ti metal–intermetallic laminate (MIL) composites. Scripta Mater 2005;52:243–8.
[18] Kattner UR, Lin JC, Chang YA. Thermodynamic assessment and calculation of the Ti–Al system. Metall Mater Trans A 1992;23:2081–90.
[19] Besser PR, Sanchez Jr JE, Alvisk R. Effect of Si on $TiAl_3$ formation in Ti/Al alloy bilayers. Mater Res Soc Symp Proc 1995;355:631–6.
[20] Zhu GL, Dai YB, Shu D, Wang J, Sun BD. Substitution behavior of Si in Al_3Ti (DO_{22}): a first-principles study. J Phys: Condens Matter 2009;21:415503–9.
[21] Ma ZP, Zhao WW, Yan JC, Li DC. Interfacial reaction of intermetallic compounds of ultrasonic-assisted brazed joints between dissimilar alloys of Ti–6Al–4V and Al–4Cu–1Mg. Ultrason Sonochem 2011;18:1062–7.
[22] Guo BG, Zhou JS, Zhang ST, Zhou HD, Pu YP, Chen JM. Tribological properties of titanium aluminides coatings produced on pure Ti by laser surface alloying. Surf Coat Technol 2008;202:4121–9.
[23] Dif R, Bes B, Ehrström JC, Sigli C, Warner TJ, Lassince P, et al. Understanding and modelling the mechanical and corrosion properties of 6056 for aerospace applications. Mater Sci Forum 2000;331–337:1613–8.
[24] Zhang F, Chen SL, Chang YA, Kattner UR. A thermodynamic description of the Ti–Al system. Intermetallics 1997;5:471–82.